Supplementary Figure 1

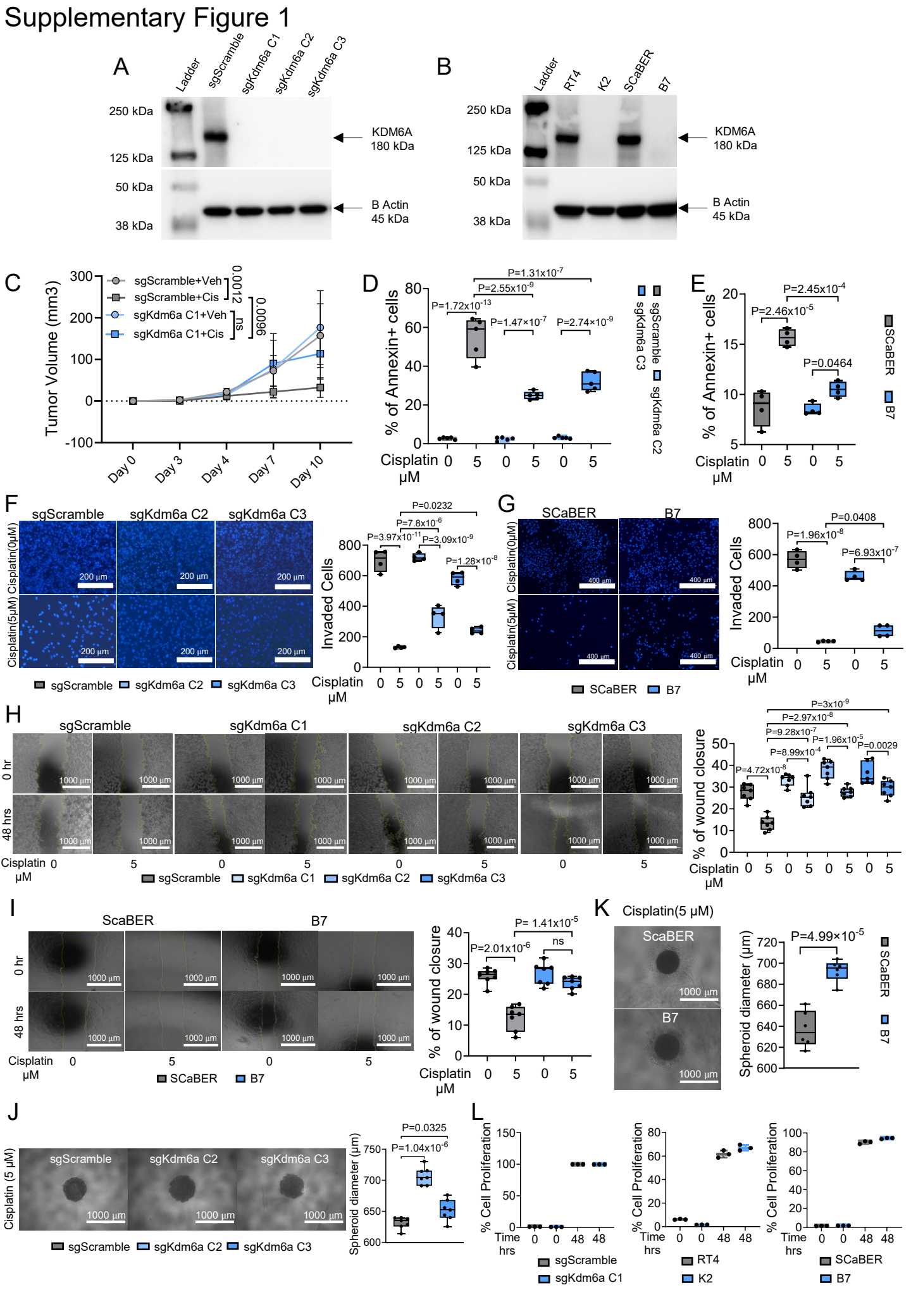

Supplementary Figure 1. Loss of KDM6A confers resistance to cisplatin treatment in bladder cancer cells. A-B. Representative images depicting KDM6A (180 kDa) and β-ACTIN (45 kDa) expression in MB49 sgScramble and sgKdm6a Clones C1, C2, C3(**A**), in RT4 with its KDM6A KO Clone K2, and in SCaBER with its KDM6A KO Clone B7(**B**). Data is representative of two independent experiments. **C.** Tumor growth curves indicating volumes of sgScramble and sgKdm6a C1 tumors from mice treated with or without cisplatin-based chemotherapy. (n=10 mice per group). P-values were calculated by Two-way ANOVA test with Tukey's correction for multiple comparisons. **D-E.** Box-and-whisker plots demonstrating percentage of Annexin positive cells in sgScramble and sgKdm6a C2, C3(**D**); in SCaBER and B7(**E**) cells, following treatment with or without 5 μM cisplatin for 48 hours (n=5(**D**) and n=4(**E**) biologically independent samples). **F-G.** Representative images (Left) and corresponding box-and-whisker plot (Right) showcasing invaded cell number in Transwell assay for sgScamble and sgKdm6a C2, C3(**F**); and SCaBER and B7(**G**) cells, treated with or without 5 μM cisplatin for 48 hours (n=4 independent visual fields). For the representative images, data is indicative of two independent experiments**.** Scale bars included. **H-I.** Representative images (Left) and box-and-whisker plot (Right) illustrating wound closure percentage in sgScramble and sgKdm6a clones(**H**), in SCaBER and B7(**I**) cells, following treatment with or without 5 μM cisplatin for 48 hours (n=7 biologically independent samples). For the representative images, data is indicative of two independent experiments. Scale bars included. **J-K**. Representative images (Left) and corresponding box-and-whisker plots (Right) comparing spheroid diameter of sgScramble and sgKdm6a C2, C3(**J**); and SCaBER and B7(**K**) treated with 5 μM cisplatin for 48 hours. (n=7(**J**) and n=6(**K**) biologically independent samples). For the representative images, data is indicative of two independent experiments. Scale bars included. **L.** Box-and-whisker-plots demonstrating percentage of cell proliferation of indicated cell lines at 0 and 48 hours (n=3 biologically independent samples). Data is representative of two independent experiments.

For **D-J,** P-values were calculated by Two-way ANOVA test with Benjamini-Hochberg correction for multiple comparisons. For **K**,Two-tailed Student's t-test was performed. For all box-and-whisker plots, center line marks the median, edges of the box represent interquartile (25th–75th) percentile and whiskers represent minimum-maximum values. Source data are provided as a Source Data file.

Supplementary Figure 2

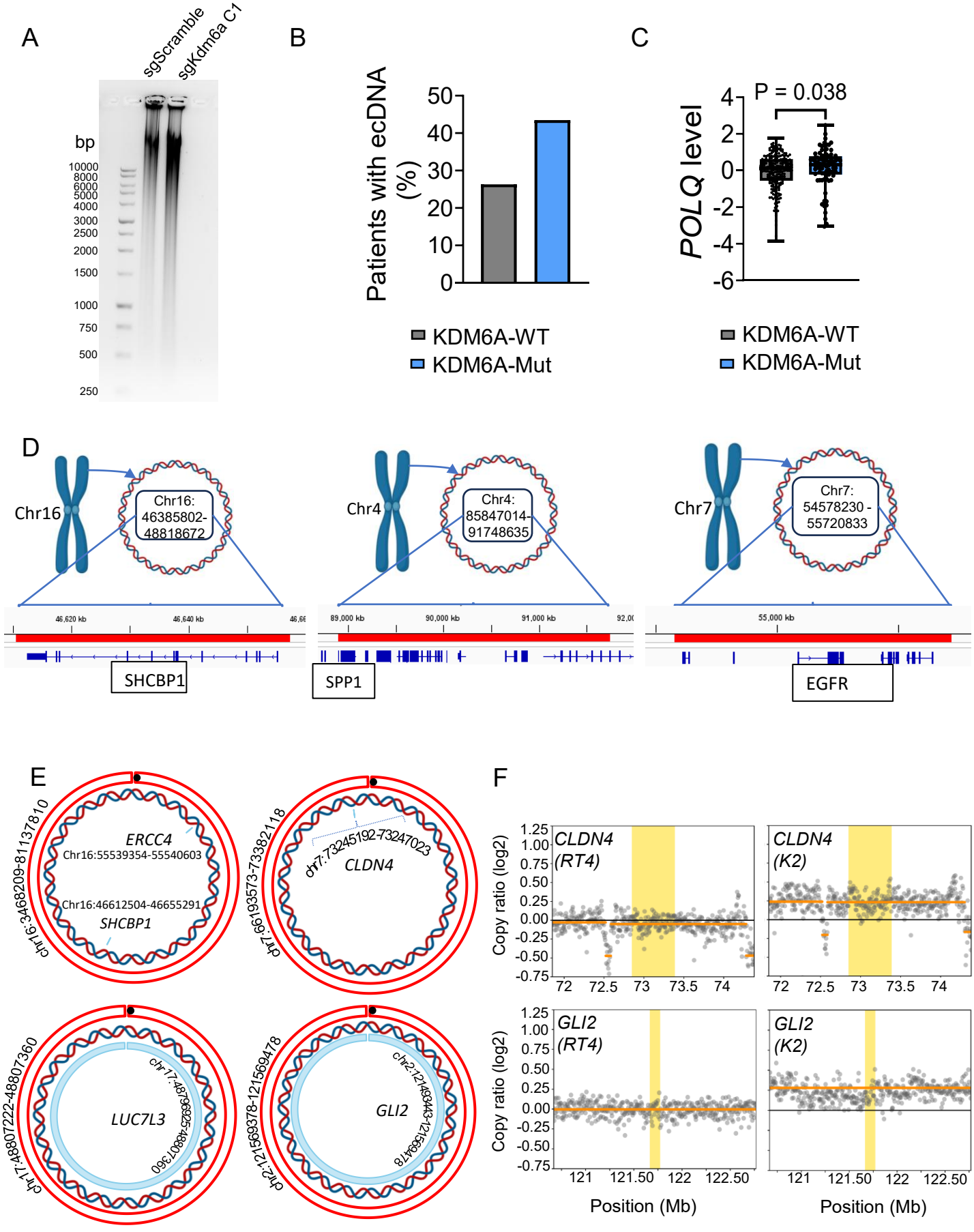

Supplementary Figure 2. KDM6A deficiency drives the accumulation of eccDNA harboring genes associated with cisplatin resistance. A. Representative electrophoresis gel image for rolling circle amplification of eccDNA from sgScramble and sgKdm6a C1 cells. Data is representative of 2 independent experiments. **B.** Bar graph showing the percentage of KDM6A-WT and KDM6A-Mut patients harboring eccDNA of the TCGA-BLCA cohort (KDM6A-WT=85, KDM6A-Mut=27 patients). **C**. Box-and-whisker plot depicting the expression of *POLQ*, in KDM6A-WT and KDM6A-Mut patients from the TCGA-BLCA cohort (n=296 patients, KDM6A-Mut=78, KDM6A-WT=218). Exact Mann-Whitney test was performed. **D.** Graphical representation and genome browser view of unique eccDNA amplicons mapped to *SHCBP1, SPP1* and *EGFR* in patients harboring KDM6A mutations from TCGA-BLCA cohort. Representative figures generated using Biorender and Integrative Genomics Viewer (IGV).Created in *BioRender. Raychaudhuri, D. (2025) https://BioRender.com/39zjkaw.* **E.** Circos plots displaying indicated eccDNA amplicons identified in K2 cells. The outer red ring represents whole amplicon, the black dot marks the start coordinate, and the inner blue region indicates segment mapped to indicated genes within the amplicon. **F.** The scatter plots show the copy number amplifications for indicated genes at their eccDNA loci in RT4 and K2 cells. The gray dots represent probes across the region labeled on x-axis, while y-axis represents the copy ratio (log2) at that genomic position for the gray dots. The orange horizontal line is the segmentation line indicating true copy number state for the segment, and the yellow vertical bars mark the indicated regions for *CLDN4* and *GLI2* within the amplicon. For all box-and-whisker plot, center line marks the median, edges of the box represent interquartile (25th–75th) percentile and whiskers represent minimum-maximum values. Source data are provided as a Source Data file.

Supplementary Figure 3

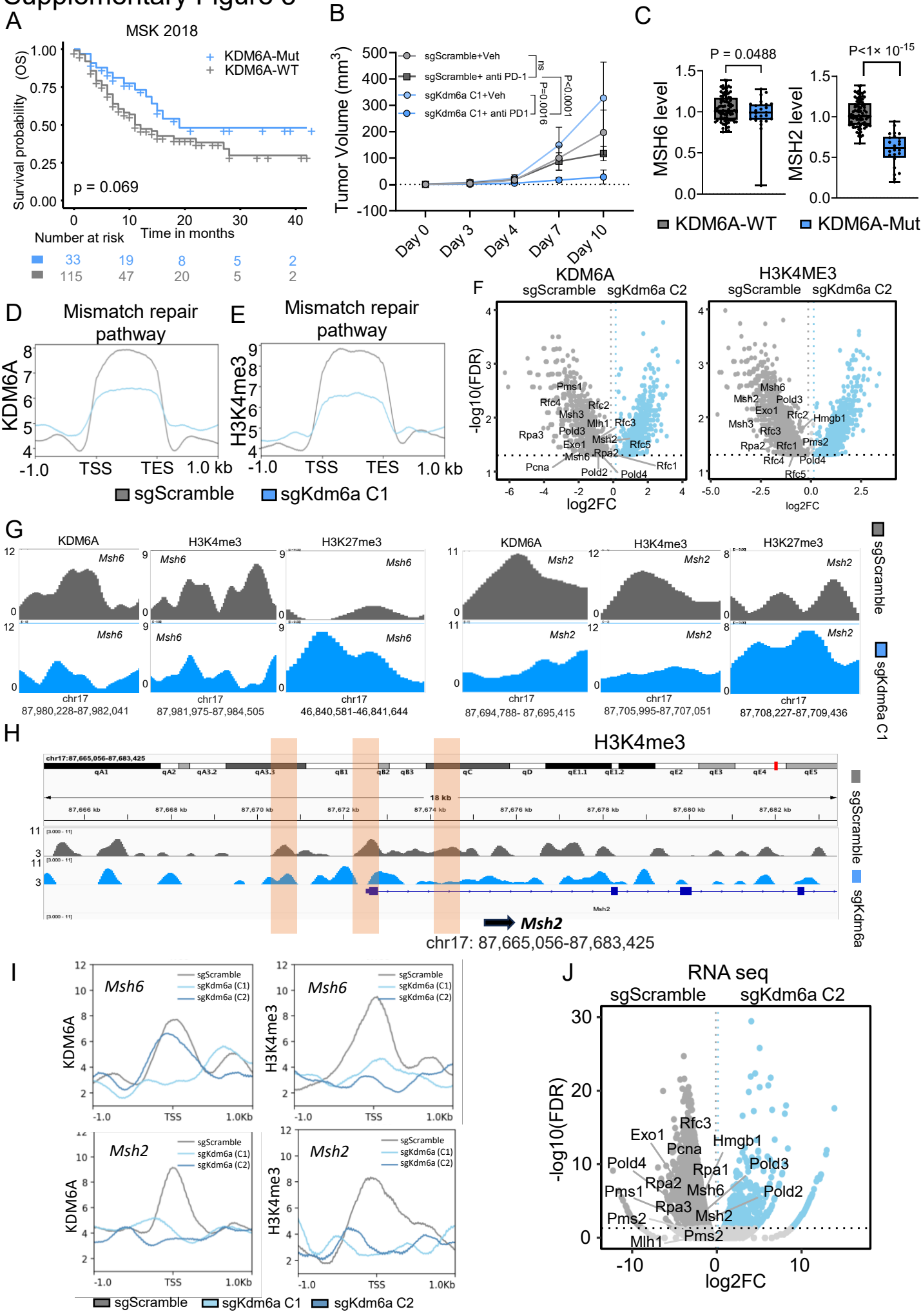

Supplementary Figure 3. Epigenetic regulation of MMR pathway genes upon KDM6A loss determines clinical response to ICT. A. Kaplan-Meier plot showing OS of KDM6A-WT and KDM6A-Mut patients receiving ICT, from MSK 2018 cohort (n=148 patients, KDM6A-Mut=33, KDM6A-WT=115). Two-tailed Log-rank test was performed. **B.** Tumor growth curves indicating sgScramble and sgKdm6a C1 tumor volumes from mice treated with and without Anti-PD-1 (n=8 mice per group). Two-way ANOVA test with Tukey's correction for multiple comparisons was performed. **C.** Box-and-whisker plots depicting expression level of MMR pathway genes between KDM6A-WT and KDM6A-Mut patients, who received immunotherapy in HCRN cohort (n=108, KDM6A-Mut=24, KDM6A-WT=84). One-tailed Student's t-test was performed. **D-E.** Profile plots depicting probability score of KDM6A(**D**) and H3K4me3(**E**) binding at ±1kb regions from TSS and TES for genes involved in MMR pathway in sgScramble and sgKdm6a C1 cells. **F**. ChIP-seq volcano plots demonstrating differential enrichment of KDM6A(Left) and H3K4me3(Right) marks in MMR genes between sgScramble and sgKdm6a C2 cells. Volcano plots show the log2 ratio of fold change (log2FC) plotted against the Absolute Confidence, -log10 adjusted p-value (log10(FDR)). P-values were calculated using the Audic-Claverie Bayesian model with MAnorm,adjusted with Benjamini–Hochberg method. **G.** Genome browser plots displaying KDM6A, H3K4me3 and H3K27me3 peaks for *Msh6* and *Msh2* gene loci in sgKdm6a and sgScramble C1 cells. The regions depicted here were identified through the differential enrichment analysis as described in (F). **H.** Genome browser plot demonstrating H3K4me3 peaks at *Msh2* gene locus in sgScramble and sgKdm6a cells. Highlighted regions indicate differential H3K4me3 enrichment between cells. **I.** Profile plots depicting probability scores of KDM6A(Left) and H3K4me3(Right) binding at promoter regions (TSS ±1kb) of indicated gene loci in sgScramble, sgKdm6a C1 and sgKdm6a C2 cells**. J**. RNA-seq volcano plot representing differential expression of MMR genes between sgScramble and sgKdm6a C2 cells. Volcano plots show the log2 ratio of fold change (log2FC) plotted against the Absolute Confidence, -log10 adjusted p-value (log10(FDR)). P-values were calculated with two tailed exact test under a negative binomial

distribution using EdgeR and adjusted with Benjamini–Hochberg method. For all box-and-whisker plots, center line marks the median, edges of the box represent interquartile (25th–75th) percentile and whiskers represent minimum-maximum values. Source data are provided as a Source Data file.

Supplementary Figure 4

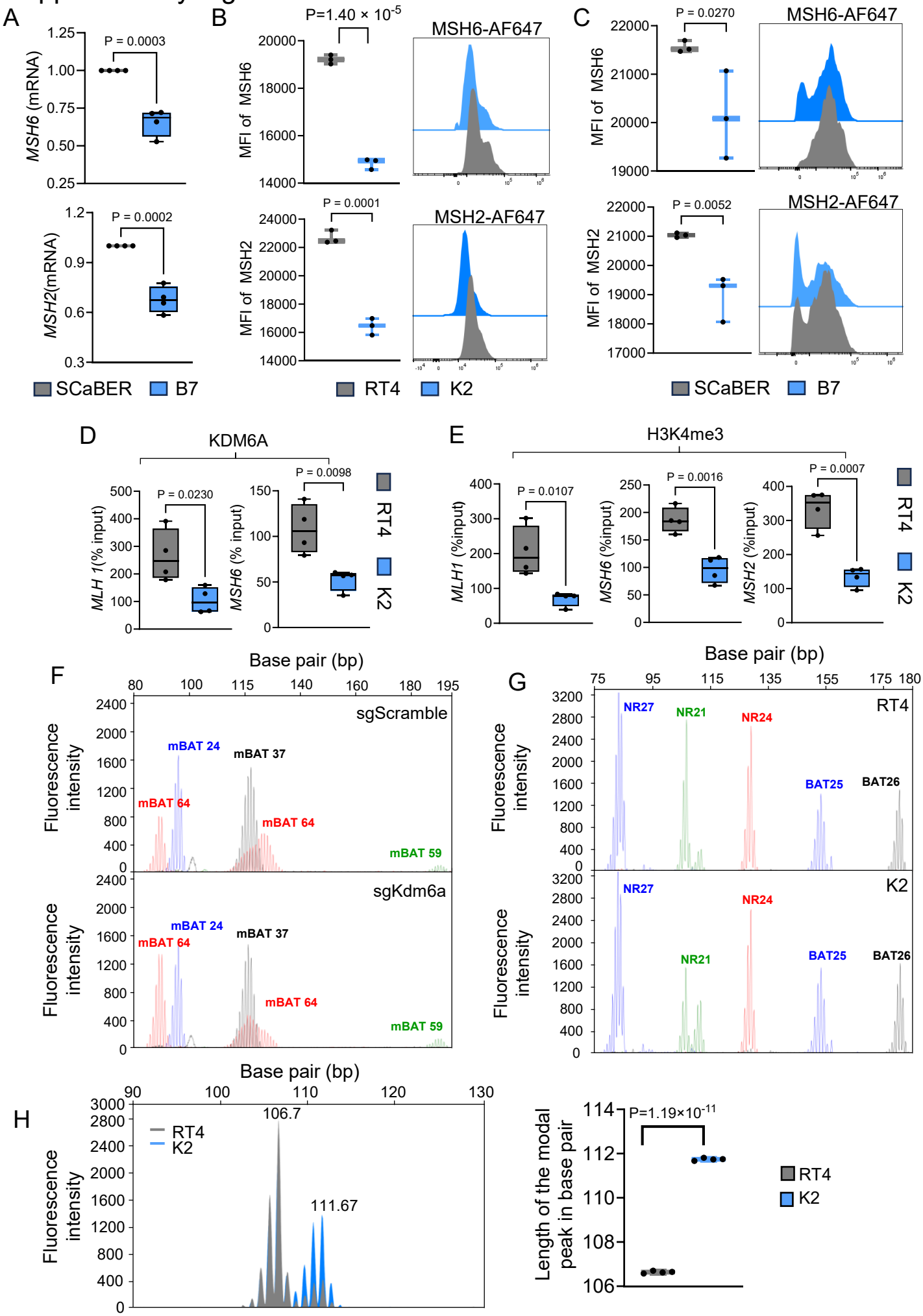

Supplementary Figure 4. Impaired MMR pathway due to KDM6A loss results in microsatellite instability. A. Box-and-whisker plots showing relative expression of *MSH6* and *MSH2* in SCaBER and B7 cells (n=4 biologically independent samples). Two-tailed Student's t-test was performed. **B-C.** Representative histograms (Left) and box-and-whisker plots (Right) showing the difference in MFI of MSH6 and MSH2 between RT4 and K2 (**B**) and SCaBER and B7 (**C**) cells (n=3 biologically independent samples). Two-tailed (**B**) and One-tailed (**C**) Student's t-test was performed. **D-E.** Box-and-whisker plots showing ChIP-qPCR analysis of KDM6A(**D**) and H3K4me3(**E**) gene enrichment at the indicated gene promoters in RT4 and K2 cell lines. (n=4 biologically independent samples). Two-tailed Student's t-test was performed. **F-G.** Representative electropherograms derived from Fragment Fluorescent Length Analysis (FFLA) of indicated microsatellite markers in sgScramble and sgKdm6a C1(**F**) cells as well as in RT4 and K2(**G**) cells. Data is representative of two independent experiments. **H.** Representative overlayed electropherogram (Left) derived from FFLA of *NR21* microsatellite from RT4 and K2 cells and corresponding box-and-whisker plot (Right) depicting the length of the modal peak in base pair in RT4 and K2 cells (n=4 biologically independent samples). Two-tailed Student's t-test was performed. Data is representative of two independent experiments. For all box-and-whisker plots, center line marks the median, edges of the box represent interquartile (25th–75th) percentile and whiskers represent minimum-maximum values. Source data are provided as a Source Data file.

Supplementary Figure 5

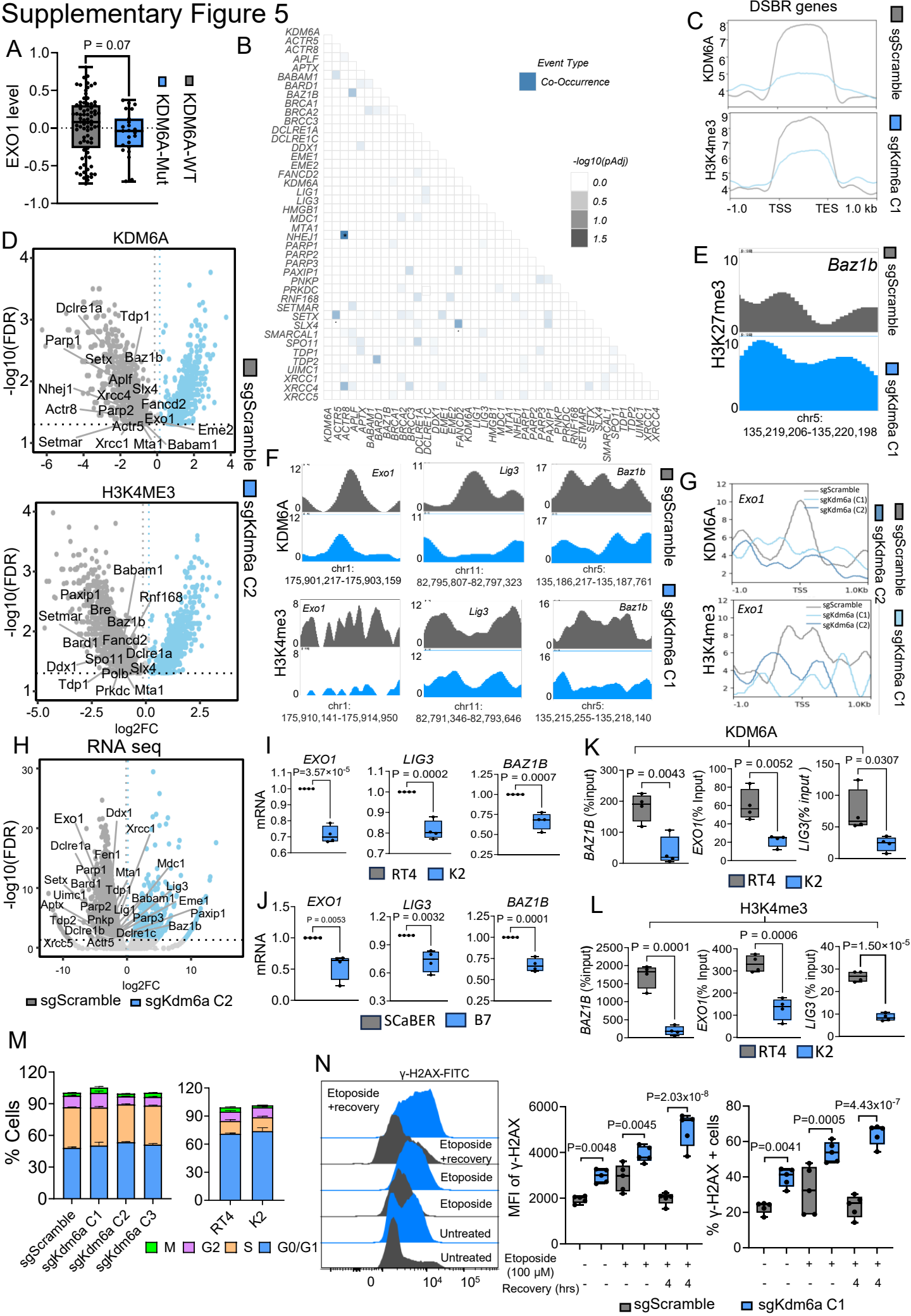

Supplementary Figure 5. Epigenetic regulation of double-stranded break repair pathway genes upon KDM6A loss. A. Box-and-whisker plots depicting *EXO1* level between KDM6A-WT and KDM6A-Mut patients in HCRN cohort (n=102 patients, KDM6A-Mut=23, KDM6A-WT=79). Mann Whitney test was performed. **B.** Somatic interaction plot depicting co-occurrence or mutual exclusivity of mutations in *KDM6A* and DSBR genes in bladder cancer patients in TCGA-BLCA cohort(N=412 patients). Two-tailed Pair wise Fisher's exact test was performed and derived p-values adjusted with Benjamini–Hochberg method (-log10(pAdj)). **C.** Profile plots representing probability score of KDM6A(Top) and H3K4me3(Bottom) binding at ±1kb regions from TSS and TES for DSBR genes in sgScramble and sgKdm6a C1 cells. **D.** ChIP-seq volcano plots demonstrating differential enrichment of KDM6A(Top) and H3K4me3(Bottom) marks in DSBR genes between sgScramble and sgKdm6a C2 cells. Volcano plots show log2 ratio of fold change (log2FC) plotted against the Absolute Confidence, -log10 adjusted p-value (log10(FDR)). P-values were calculated using the Audic-Claverie Bayesian model with MAnorm, adjusted with Benjamini–Hochberg method. **E.** Genome browser plots depicting H3K27me3 peaks for *Baz1b* gene loci in sgScramble and sgKdm6a C1 cells. Regions were identified through differential enrichment analysis. **F.** Genome browser plots depicting KDM6A(Top) and H3K4me3(Bottom) peaks at *Exo1*, *Lig3* and *Baz1b* loci in sgScramble and sgKdm6a C1 cells. Regions were identified through differential enrichment analysis as described in (D). **G.** Profile plots depicting probability scores of KDM6A(Top) and H3K4me3(Bottom) binding at *Exo1* promoter region (TSS ±1kb) in sgScramble, sgKdm6a C1 and sgKdm6a C2 cells**.** **H.** RNA-seq volcano plot representing differential expression of DSBR genes between sgScramble and sgKdm6a C2 cells. Volcano plots show log2 ratio of fold change (log2FC) plotted against the Absolute Confidence, -log10 adjusted p-value (log10(FDR)). P-values were calculated with two-tailed exact test under a negative binomial distribution using EdgeR and adjusted with Benjamini–Hochberg method. **I-J.** Box-and-whisker plots showing relative expression of indicated genes in RT4 and K2(**I**) and SCaBER and B7(**J**) cells (n=4 biologically independent samples). **K-L.** Box-and-whisker plots showing ChIP-qPCR analysis of KDM6A (**K**)

and H3K4me3(**L**) gene enrichment at indicated gene promoters in RT4 and K2 cells (n=4 biologically independent samples). **M**. Stacked bar plots depicting cell cycle distribution in sgScramble and sgKdm6a clones(Left), RT4 and K2 cells(Right) (n=3 biologically independent samples). Data representative of two independent experiments. **N.** Representative histogram(Left) and box-and-whisker plots indicating MFI(Middle) and percentage(Right) of gamma-H2AX positive sgScramble and sgKdm6a C1 cells treated with or without 100μM Etoposide and 4 hours of recovery or no recovery (n=5 biologically independent samples). For **I-L,** Two-tailed Student's t-test was performed. For **N**, P-values were calculated by Two-way ANOVA test with Benjamini-Hochberg correction for multiple comparisons. For all box-and-whisker plots, center line marks the median, edges of the box represent interquartile (25th–75th) percentile and whiskers represent minimum-maximum values. Source data are provided as a Source Data file.

Supplementary Figure 6

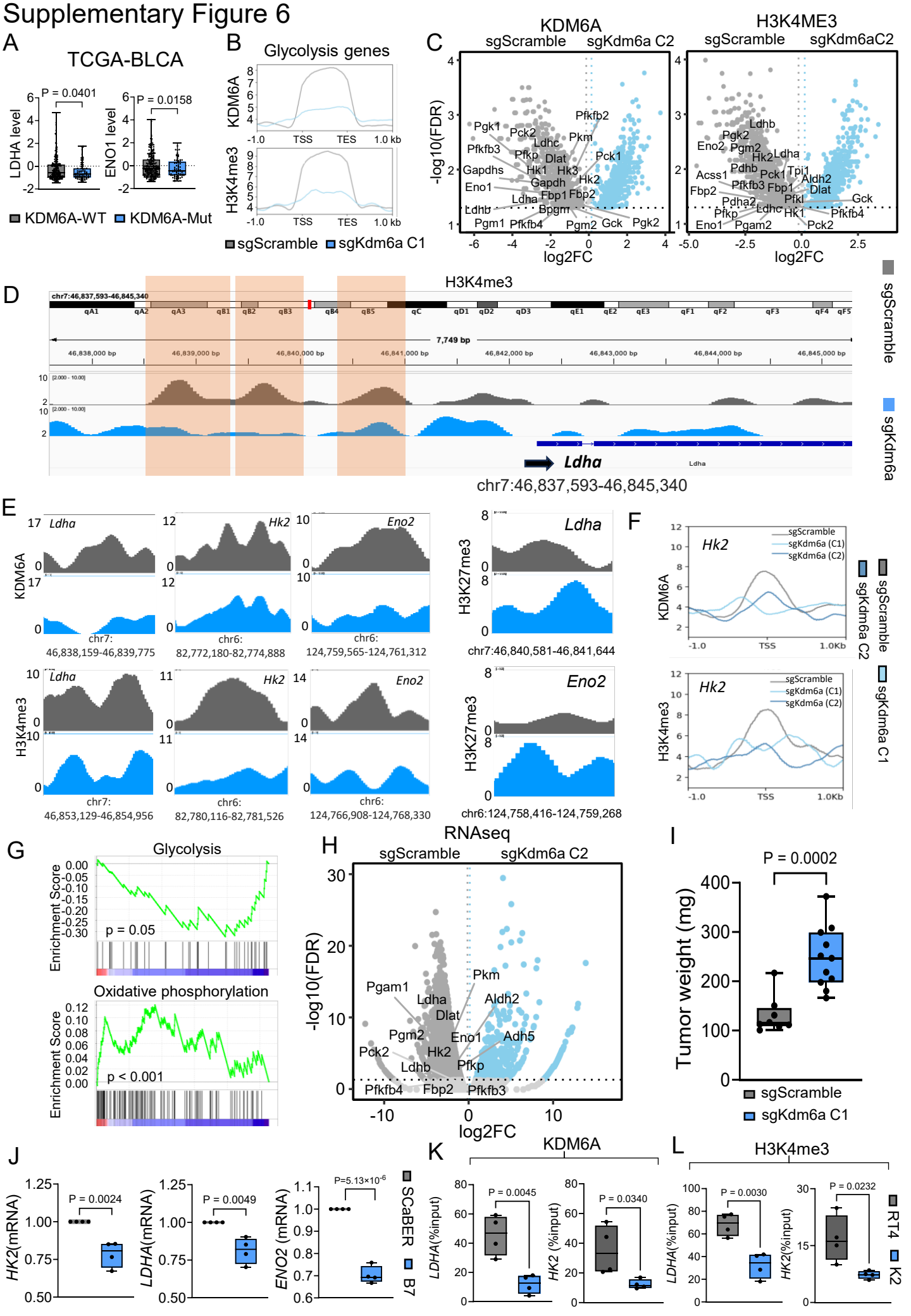

Supplementary Figure 6. KDM6A regulates the lactate output by altering the epigenetic landscape of glycolytic genes. **A.** Box-and-whisker plots depicting expression of genes involved in glycolysis and lactate production in KDM6A-WT and KDM6A-Mut patients, from TCGA dataset (n=293 patients, KDM6A-Mut=76, KDM6A-WT=217). One-tailed Student's t-test was performed. **B.** Profile plots representing probability score of KDM6A(Top) and H3K4me3(Bottom) binding at ±1kb regions from TSS and TES for glycolysis and lactate production pathway genes in sgScramble and sgKdm6a C1 cell lines. **C.** ChIP-seq volcano plots demonstrating differential enrichment of KDM6A(Left) and H3K4me3(Right) marks in indicated glycolysis genes between sgScramble and sgKdm6a C2 cells. Volcano plots show log2 ratio of fold change (log2FC) plotted against the Absolute Confidence, -log10 adjusted p-value (log10(FDR)). P-values were calculated using the Audic-Claverie Bayesian model with MAnorm, adjusted with Benjamini–Hochberg method. **D.** Genome browser plot demonstrating H3K4me3 peaks at *Ldha* gene locus in sgScramble and sgKdm6a cells. Highlighted regions indicate differential H3K4me3 enrichment between cells. **E.** Genome browser plots displaying KDM6A, H3K4me3 and H3K27me3 peaks for indicated gene loci in sgKdm6a and sgScramble C1 cells. Regions depicted were identified through differential enrichment analysis as described in (C). **F.** Profile plots indicating probability scores of KDM6A(Top) and H3K4me3(Bottom) binding at promoter regions (TSS ±1kb) of *Hk2* gene loci in sgScramble, sgKdm6a C1 and sgKdm6a C2 cells. **G.** Plots representing indicated GSEA pathways generated from genes with KDM6A enrichment in sgKdm6a C1 cells compared to sgScramble cells. Indicated p-values represent one-tailed nominal p-value of gene enrichments calculated by permutations. **H.** RNA-seq volcano plot representing differential expression of the glycolysis genes between sgScramble and sgKdm6a C2 cells. Volcano plots show log2 ratio of fold change (log2FC) plotted against the Absolute Confidence, -log10 adjusted p-value (log10(FDR)). P-values were calculated with two tailed exact test under a negative binomial distribution using EdgeR and adjusted with Benjamini–Hochberg method.

I. Box-and-whisker plots demonstrating sgScramble and sgKdm6a C1 tumor weights (n=8 sgScramble and n=11 sgKdm6a C1 tumor bearing mice). **J**. Box-and-whisker plots showing relative expression of indicated genes in SCaBER and B7 cells (n=4 biologically independent samples). **K-L**. Box-and-whisker plots depicting ChIP-qPCR analysis of KDM6A(**K**) and H3K4me3(**L**) gene enrichment at the indicated gene promoters in RT4 and K2 cells (n=4 biologically independent samples). For **I-L**, Two-tailed Student's t-test was performed. For all box-and-whisker plots, center line marks the median, edges of the box represent interquartile (25th-75th) percentile and whiskers represent minimum-maximum values. Source data are provided as a Source Data file.

Supplementary Figure 7

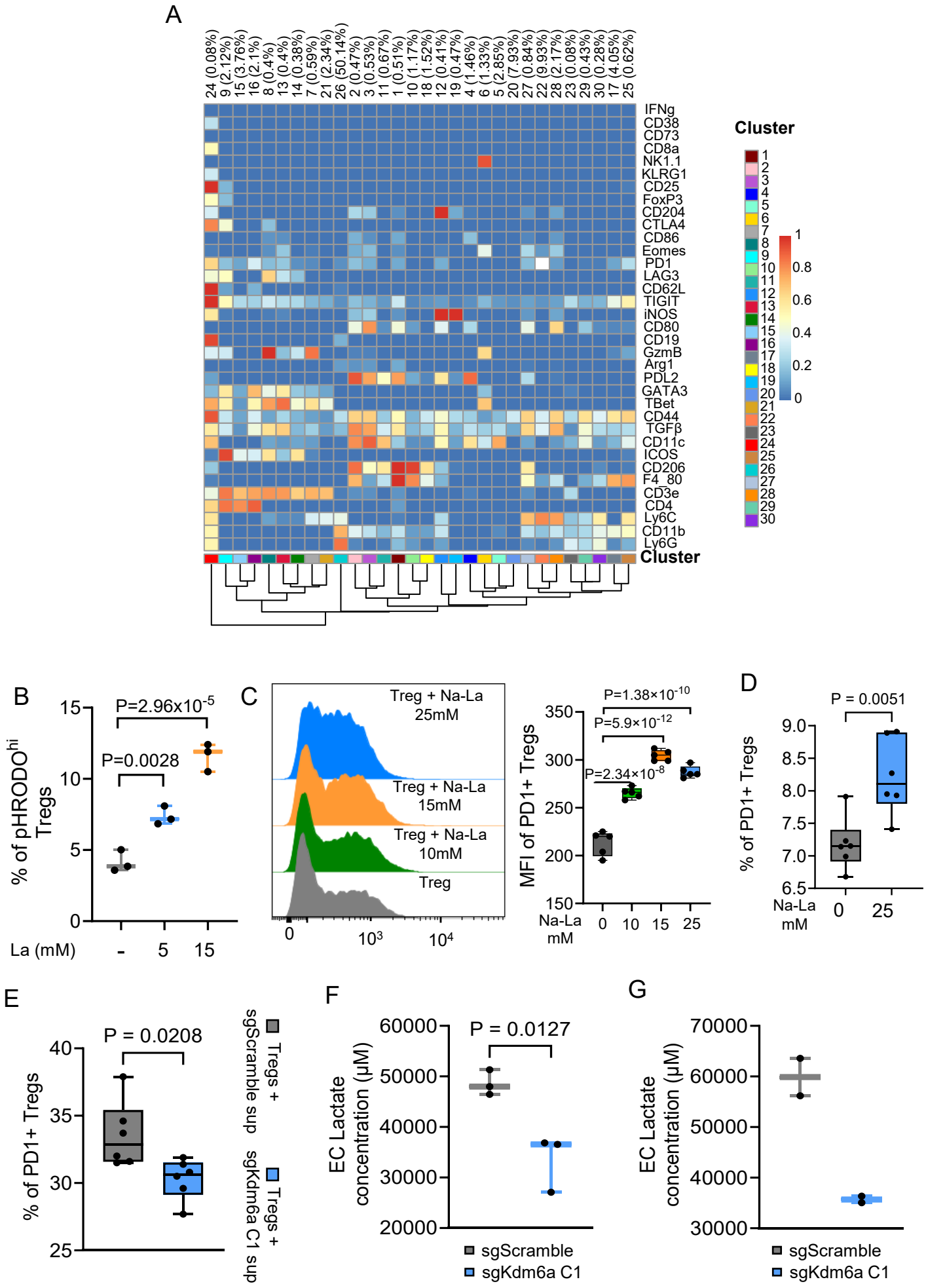

Supplementary Figure 7. Deficiency of KDM6A attenuates lactate production in Tregs. A. Heatmap indicating the expression of protein markers of interest in the different $CD45^+$ immune cell clusters (shown in Fig. **5A**) as determined by mass cytometry. (n=4 mice per group) **B.** Box-and-whisker plot representing the percentage of $pHRODO^{hi}$ cells in *in-vitro* generated Tregs treated with or without 5mM and 15mM Lactic acid (La) for 30 minutes (n=3 biologically independent samples). **C.** Representative histogram (Left) and box-and-whisker plot (Right) depicting the MFI of PD-1 in *in-vitro* generated untreated Tregs and Tregs treated with indicated doses of Na-La (n=5 biologically independent samples). **D.** Box-and-whisker plot demonstrating the percentage of PD-1 positive cells in *in-vitro* generated Tregs treated with and without 25 mM Na-La for 48 hours (n=6 biologically independent samples). **E.** Box-and-whisker plot showing the percentage of PD-1 positive cells in *in-vitro* generated Tregs treated with the culture supernatants from sgScramble or sgKdm6a C1 cell lines for 24 hours (n=6 biologically independent samples). **F.** Box-and-whisker plot depicting the EC L-Lactate concentration in the supernatant of sgScramble and SgKdm6a C1 cells cultured for 24 hours (n=3 biologically independent samples). These supernatants were subsequently utilized to treat the Tregs in Figure 5H and S7E. **G.** Box-and-whisker plot displaying the EC L-Lactate concentration in the supernatant of sgScramble and SgKdm6a C1 cell lines cultured for 36 hours (n=2 biologically independent samples). These supernatants were subsequently utilized to treat the Tregs in Figure 5I. For **B-C,** P-values were calculated by One-way ANOVA test with Benjamini-Hochberg correction for multiple comparisons. For **D-F,** Two-tailed Student's t-test was performed. For all box-and-whisker plots, center line marks the median, edges of the box represent interquartile (25th–75th) percentile and whiskers represent minimum-maximum values. Source data are provided as a Source Data file.

Supplementary Figure 8

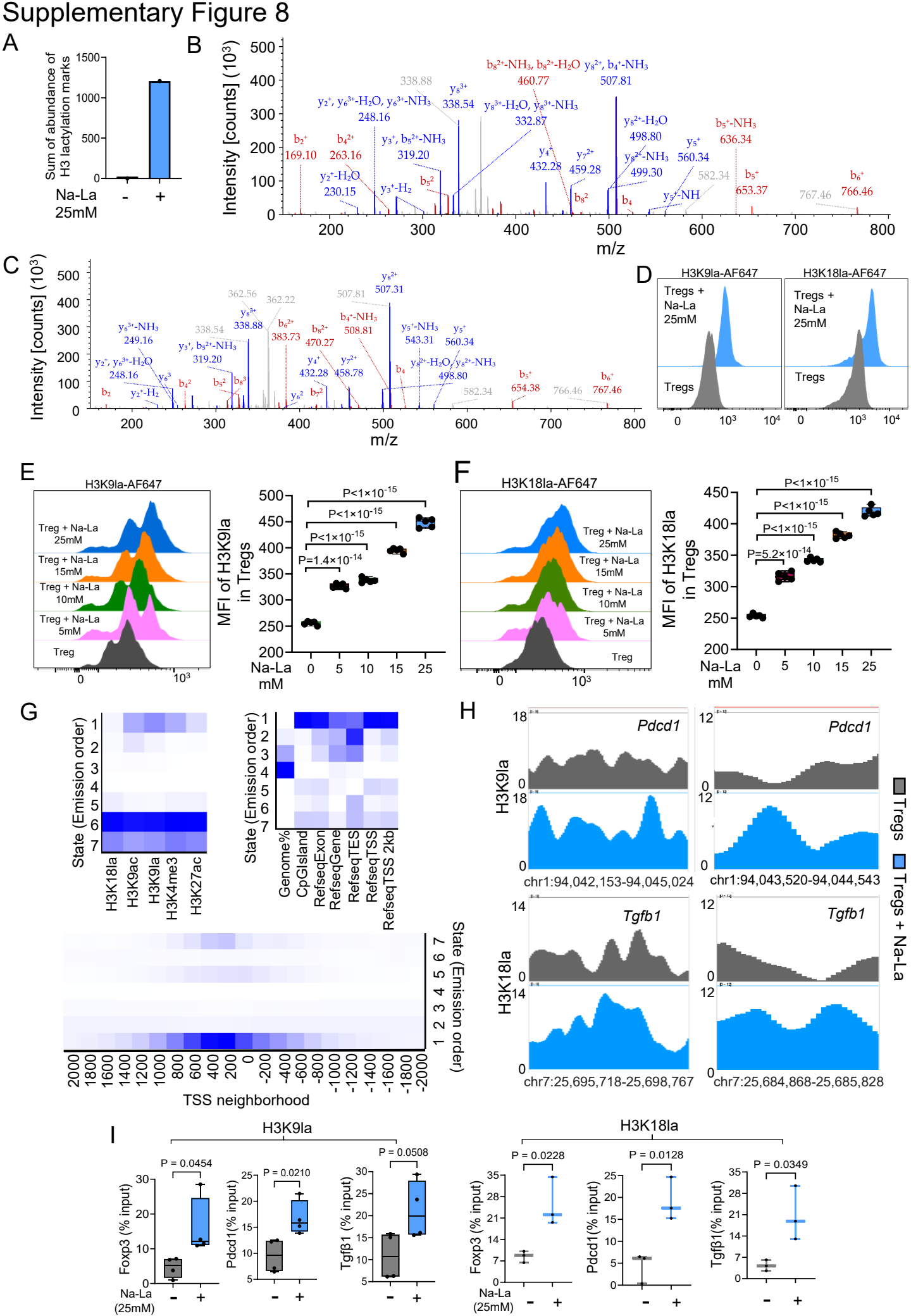

Supplementary Figure 8. Exogenous lactate reprograms *in-vitro* Tregs by inducing Histone H3 Lysine lactylation (H3Kla). A. Bar plot illustrating the sum of abundance of H3 lactylation marks in *in-vitro* generated Tregs treated with and without 25 mM ^{13}C labelled Na-La for 48 hours as determined by high-performance liquid chromatography (HPLC)–tandem mass spectrometry (MS/MS) analysis. **B-C.** MS/MS spectra of H3K18la in *in-vitro* generated untreated Tregs**(B)** and Tregs treated with 25 mM ^{13}C labelled Na-La**(C)** for 48 hours. **D.** Representative histogram depicting the MFI of H3K9la(Left) and H3K18la(Right) in *in-vitro* generated Tregs treated with and without 25 mM Na-La for 48 hours as shown in Fig **6A** (n=3 biologically independent sample per group). **E-F.** Representative histograms (Left) and box-and-whisker plots (Right) depicting the MFI of H3K9la(**E**) and H3K18la(**F**) in *in-vitro* generated untreated Tregs and Tregs treated with indicated doses of Na-La (n=5 biologically independent samples). P-values were calculated by One-way ANOVA test with Benjamini-Hochberg correction for multiple comparisons. **G.** Heatmap indicating emission parameters, generated from ChromHMM analysis. Each row corresponds to a specific chromatin state and each column corresponds to a specific epigenetic mark in *in-vitro* generated Tregs(Left). Heatmap displaying the fold enrichment of different chromatin states in distinct genomic regions based on the indicated epigenetic marks in *in-vitro* generated Tregs(Right). Heatmap demonstrating the fold enrichment of different chromatin states around transcription start sites (TSS) based on indicated epigenetic marks, in *in-vitro* generated Tregs(Bottom). The darker blue color corresponds to a greater probability of observing the mark in the state. **H.** Genome browser plots displaying H3K9la(Left) and H3K18la(Right) peaks for indicated gene loci in *in-vitro* generated Tregs treated with and without 25 mM Na-La for 48 hours. The regions depicted here were identified through the differential enrichment analysis. **I.** Box-and-whisker plots demonstrating the ChIP qPCR analysis of H3K9la(Left) and H3K18la(Right) enrichment at the indicated gene promoters in *in-vitro* generated Tregs treated with and without 25 mM Na-La for 48 hours. Data is represented as

percentage of input (n=4(Left) and n=3(Right) biologically independent samples). Two tailed Student's t-test was performed. For all box-and-whisker plots, center line marks the median, edges of the box represent interquartile (25th–75th) percentile and whiskers represent minimum-maximum values. Source data are provided as a Source Data file.

Supplementary Figure 9

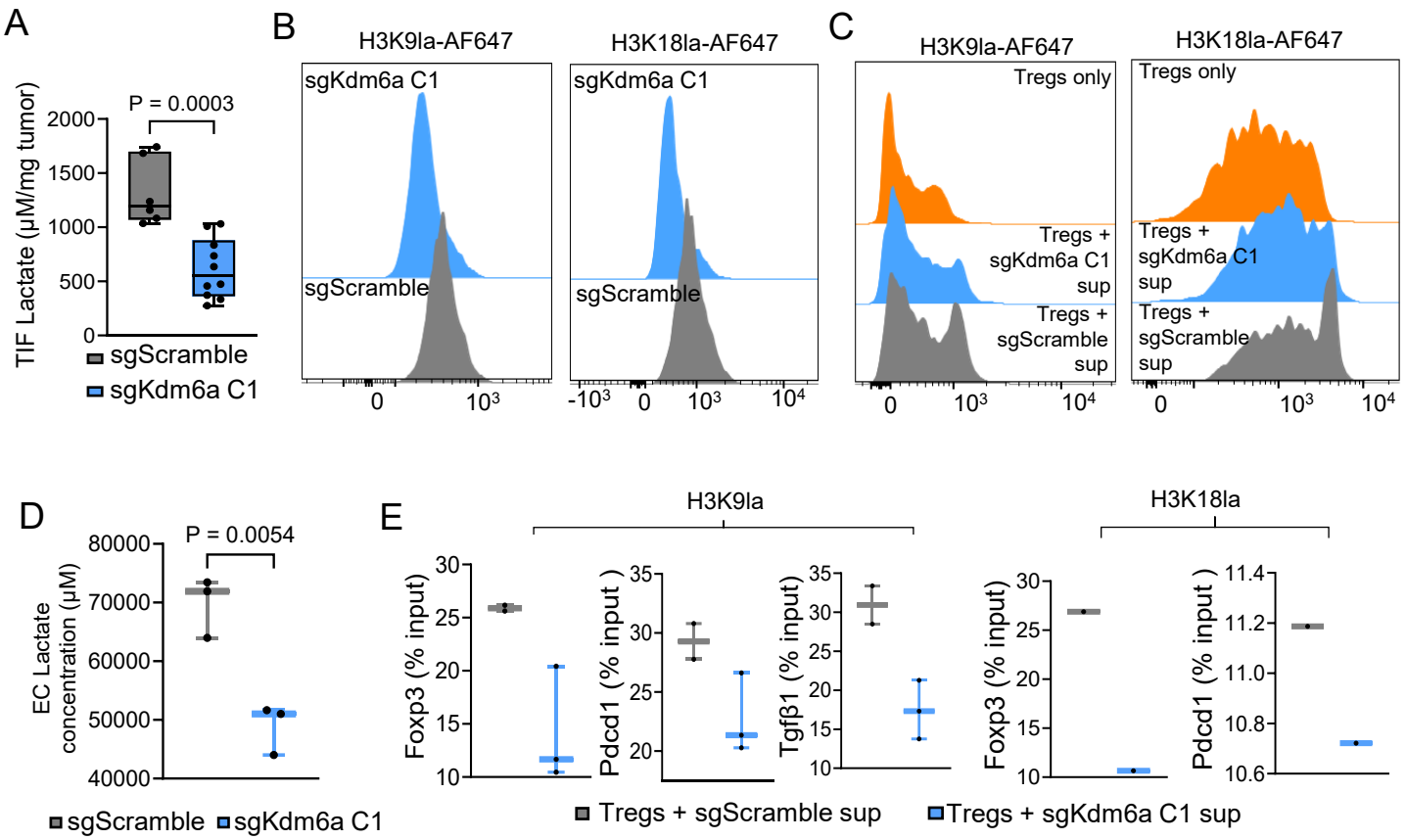

Supplementary Figure 9. KDM6A loss mediated reduction in intratumoral lactate modulates critical Treg specific genes. A. Box-and-whisker plot showing the L-lactate concentrations in the TIF normalized to corresponding tumor weights, obtained from sgScramble and sgKdm6a C1 tumors (n=6 sgScramble and n=10 sgKdm6a C1 tumor bearing mice). Two-tailed Student's t test was performed. **B.** Representative histograms displaying the MFI of H3K9la Left) and H3K18la(Right) in Intratumoral Tregs derived from sgScramble and sgKdm6a C1 tumor harboring mice. **C.** Representative histograms representing the MFI of H3K9la(Left) and H3K18la(Right) in *in-vitro* generated Tregs treated with and without culture supernatants from sgScramble and sgKdm6a C1 cell lines for 24 hours. **D.** Box-and-whisker plot depicting the EC L-Lactate concentration in the supernatants of sgScramble and sgKdm6a cell lines, measured following 24 hours of culture (n=3 biologically independent samples). These supernatants were subsequently utilized to treat the Tregs in Figure 6F, 6G, S9C and S9E. Two-tailed Student's t-test was performed. **E.** Box-and-whisker plots showing the ChIP qPCR analysis of H3K9la(Left) and H3K18la(Right) enrichment at the indicated gene promoters in *in-vitro* generated Tregs treated with culture supernatants from sgScramble and sgKdm6a C1 cell lines for 24 hours (n=2(Left) and n=1(Right) biologically independent samples). For all box-and-whisker plots, center line marks the median, edges of the box represent interquartile (25th–75th) percentile and whiskers represent minimum-maximum values. Source data are provided as a Source Data file.

Supplementary Figure 10

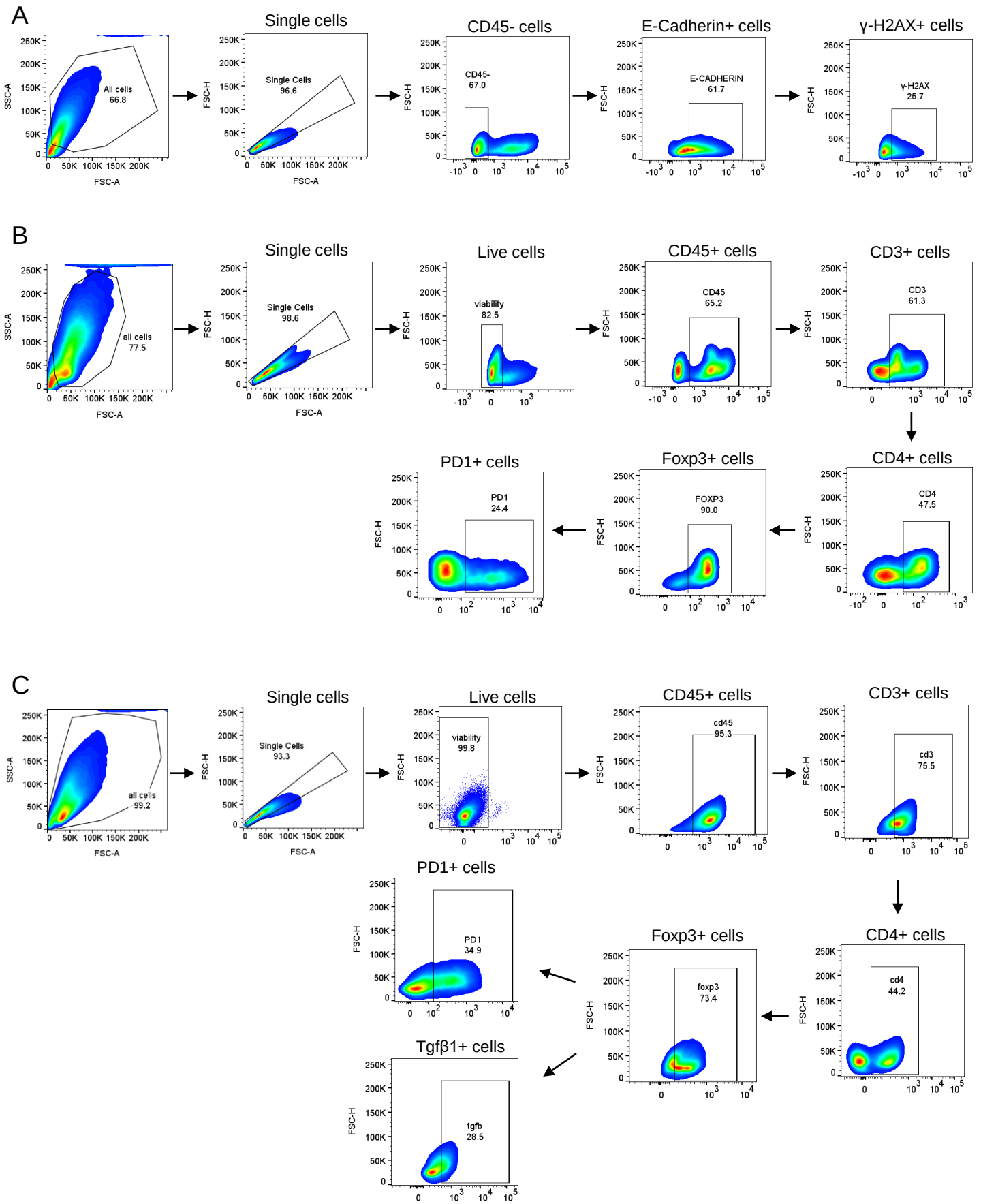

Supplementary Figure 10 A. Pseudo color plots demonstrating the gating strategy to analyze the γ-H2AX % in MB49 sgScramble and sgKDM6A C1 tumors as mentioned in Figure 3F. **B.** Pseudo color plots demonstrating the gating strategy for PD1+ intratumoral Tregs population in sgScramble and sgKdm6a C1 tumors as shown in Figure 5D,6E and Supplementary Figure 9B. **C.** Pseudo color plots demonstrating the gating strategy for Foxp3 cell populations in *in-vitro* generated Tregs as shown in Figure 5G,5H,6A,F and Supplementary Figure 7C,7D,7E,8D,8E,8F,9C.

Supplementary Table 1

REAGENT or RESOURCE	SOURCE	IDENTIFIER	Dilution
Antibodies			
KDM6A / UTX Primary Antibody (Clone D3Q1I)	Cell Signaling Technology	Cat# 33510, RRID: AB_2721244	1:2000
Beta Actin Rabbit Secondary Antibody	Cell Signaling Technology	Cat# 4967, RRID: AB_330288	1:2000
Anti-Mouse CD45 Antibody (Clone 30-F11)	Standard BioTools	Cat# 3089005B, RRID: AB_2651152	1:200
KLRG1	Millipore Sigma	Cat#MABF467, clone2F1	1:200
Anti-Mouse CD11c Antibody (Clone N418)	Standard BioTools	Cat# 3142003B, RRID: AB_2814737	1:50
Anti-mouse CD4 Antibody (Clone RM4-5)	BioLegend	Cat# 100561, RRID: AB_2562762	1:200
Anti-mouse CD62L Antibody (Clone MEL-14)	BioLegend	Cat# 104402, RRID: AB_313089	1:100
Anti-mouse CD73 Antibody (Clone TY/23)	BioLegend	Cat# 117202, RRID: AB_2936539	1:400
Anti-Mouse CD8a Antibody (Clone 53-6.7)	Standard BioTools	Cat# 3146003B, RRID: AB_2687833	1:100
Anti-mouse Ly-6G Antibody (Clone 1A8)	BioLegend	Cat# 127637, RRID: AB_2563784	1:200
Anti-Mouse CD11b Antibody (Clone M1/70)	Standard BioTools	Cat# 3148003B, RRID: AB_2814738	1:1600
Anti-Mouse CD19 Antibody (Clone 6D5)	Standard BioTools	Cat# 3149002B, RRID: AB_2814679	1:200
Anti-Mouse Ly-6C Antibody (clone HK1.4)	Standard BioTools	Cat# 3150010B, RRID: AB_2895118	1:400

Anti- CD25 Antibody (Clone 3C7)	Standard BioTools	Cat# 3151007B, RRID: AB_2827880	1:50
Anti-Mouse CD3e Antibody (Clone 145-2C11)	Standard BioTools	Cat# 3152004, RRID: AB_2687836	1:100
TIGIT, clone 1G9	Millipore Sigma	Cat#MABF2657	1:50
CTLA-4, clone UC10-4B9	Standard BioTools	Cat#3154008B	1:100
Anti-T-bet Antibody (Clone 4B10)	BioLegend	Cat# 644825, RRID: AB_2563788	1:150
Anti-human/mouse Granzyme B Recombinant Antibody (Clone QA16A02)	BioLegend	Cat# 372202, RRID: AB_2686929	1:50
Anti-Mouse Foxp3 Antibody (Clone FJK-16s)	Standard BioTools	Cat# 3158003A, RRID: AB_2814740	1:100
PD-1, clone J43	Standard BioTools	Cat#3159023B,	1:100
Anti-mouse CD38 Antibody (clone 90)	BioLegend	Cat# 102702, RRID: AB_312923	1:400
Anti-Mouse iNOS Antibody (Clone CXNFT)	Standard BioTools	Cat# 3161011B, RRID: AB_2922920	1:100
Anti-mouse CD204 (Clone 7G5C33)	BioLegend	Cat# 676202, RRID: AB_2565623	1:100
Anti-mouse CD273/PD-L2 (Clone TY25)	BioLegend	Cat# 107202, RRID: AB_345250	1:100
Anti-Mouse LAP/TGFb Antibody (Clone TW7-16B4)	Standard BioTools	Cat# 3164014, RRID: AB_2687842	1:200
Anti-mouse IFN-γ (Clone XMG1.2)	BioLegend	Cat# 505843, RRID: AB_2562847	1:75
EOMES Monoclonal Antibody (Clone Dan11mag)	Thermo Fisher Scentific	Cat# 14-4875-82, RRID: AB_11042577	1:150

CD80 Monoclonal Antibody (Clone 16-10A1)	Thermo Fisher Scentific	Cat# 14-0801-82, RRID: AB_467346	1:800
Arginase I Antibody (Clone 8C9)	Santa Cruz Biotechnology	Cat# sc-47715, RRID: AB_626697	1:300
Anti-Mouse CD206/MMR (Clone C068C2)	Standard BioTools	Cat# 3169021B, RRID: AB_2832249	1:75
Anti-Mouse NK1.1 Antibody (Clone PK136)	Standard BioTools	Cat# 3170002B, RRID: AB_2885023	1:100
Anti-Human/Mouse CD44 (Clone IM7)	Standard BioTools	Cat# 3171003B, RRID:AB_2895121	1:400
Gata-3 Monoclonal Antibody (Clone TWAJ)	Thermo Fisher Scentific	Cat# 14-9966-82, RRID: AB_1210519	1:100
Anti Mouse CD278/ICOS	BioLegend	Cat# 117408, RRID: AB_2122603	1:100
LAG3, clone C9B7W	Standard BioTools	Cat#3174019B	1:100
F4/80 Monoclonal Antibody (Clone BM8)	Thermo Fisher Scentific	Cat# 14-4801-82, RRID: AB_467558	1:100
Anti-mouse CD86 Antibody (Clone GL-1)	BioLegend	Cat# 105001, RRID: AB_313144	1:100
Rabbit Anti-mouse EXO1	Bioss	Cat#BS-13119R	1:200
Mouse Anti-Phospho-Histone H2A.X (Ser 139)	Abcam	Cat#ab242296	1:100
Goat anti-mouse FITC-conjugated secondary	Abcam	Cat#ab242296	1:100
H3K4me3 Histone antibody	Active Motif	Cat#39159, RRID:AB_2615077	10µg per pull down

			reaction
H3K27ac Histone antibody	Active Motif	Cat#39133, RRID:AB_2561016	10µg per pull down reaction
H3K27me3 Histone antibody	Active Motif	Cat#39155, RRID:AB_2561020	10µg per pull down reaction
H3K9la Histone Antibody (Clone 13H2L1)	PTM-BIO	Cat# PTM-1419RM, RRID:AB_3076695	10µg per pull down reaction
H3K18la Histone Antibody (Clone 22h2L3)	PTM-BIO	Cat# PTM-1406RM, RRID:AB_2909438	10µg per pull down reaction
H3K9ac Histone antibody	Active Motif	Cat#39137, RRID:AB_2561017	10µg per pull down reaction

Anti-mouse MSH2 Antibody (Clone 2L9I4) conjugated in-house with AF647	Bio-Techne	Cat #NBP3-16692	1:50
Anti-mouse MSH6 Antibody (Clone 035) conjugated in-house with AF647	Bio-Techne	Cat # NBP2-89265	1:50
Purified Anti-Mouse CD16/CD32 (Mouse BD Fc Block) Clone 2.4G2	BD Biosciences	Cat # 553142, RRID:AB_394657	1:200
Annexin V Pacific Blue	ThermoFisher Scientific	Cat # A35122	1:20
Alexa Fluor 532 anti-mouse CD45 Antibody (Clone 30-F11)	eBioscience	Cat # 58-0451-82, RRID:AB_11218871	1:50
Alexa Fluor 488 anti-mouse CD3 Antibody (Clone 17A2)	BioLegend	Cat# 100210, RRID:AB_493530	1:50
Alexa Fluor 700 anti-mouse CD4 Antibody (Clone RM4-5)	BioLegend	Cat# 100536,RRID:AB_493701	1:50
Brilliant Violet 650 anti-mouse CD25 Antibody (Clone PC61)	BioLegend	Cat# 102038, RRID: AB_2563060	1:50
PerCP-Cyanine5.5 anti-mouse FOXP3 Antibody (Clone FJK-16s)	eBioscience	Cat# 45-5773-82, RRID: AB_914351	1:25
Brilliant Violet 605 anti-Mouse PD-1 (Clone J43)	BD Biosciences	Cat # 563059, RRID: AB_2737980	1:50
Brilliant Violet 421 anti-mouse TGF-β1 Antibody (Clone TW7-16B4)	BioLegend	Cat# 141407, RRID:AB_2561580	1:25

H3K9la Histone Antibody (Clone 13H2L1) conjugated in-house with AF647	PTM-BIO	Cat# PTM-1419RM, RRID:AB_3076695	1:100
H3K18la Histone Antibody (Clone 22h2L3) conjugated in-house with AF647	PTM-BIO	Cat# PTM-1406RM, RRID:AB_2909438	1:100
Pacific Blue anti-mouse CD45 (Clone 30-F11)	BioLegend	Cat#103126, RRID: AB_493535	1:50
Phycoerythrin anti-mouse E-Cadherin (Clone 4A2)	Cell Signaling Technology	Cat#82718, RRID: AB_2799998	1:50
Anti-PD-1 (Clone RMP1-14)	Bio X Cell	Cat# BE0146, RRID: AB_10949053	200 µg, 100 µg, and 100 µg
Anti-mouse CD3e Clone: 145-2C11	BD Biosciences	Cat # 553057, RRID: AB_394590	3 µg/ml
Anti-mouse CD28 Clone: 37.51	BD Biosciences	Cat # 553294, RRID: AB_394763	2 µg/ml
Pan Anti-Kla Antibody (Anti-L-Lactyllysine Rabbit pAb)	PTM BIO	Cat #PTM-1401, RRID:AB_2868521	10µg per pull down reaction
Experimental Models: Cell Lines			
MB49 Mouse Bladder Carcinoma Cell Line	Sigma Aldrich	Cat#SCC148	

sgScramble	MDACC Functional Genomics Core	N/A	
sgKdm6a C1-C3	MDACC Functional Genomics Core	N/A	
RT4	ATCC	Cat#HTB-2	
K2	Generated in collaboration with Dr. Byron H. Lee		
SCaBER	ATCC	Cat#HTB-3	
B7	Generated in collaboration with Dr. Byron H. Lee		
Experimental Models: Mouse			
Mouse line	Company	Catalog number	Age
C57BL/6	NCI	556C57BL/6NCr	5-7 weeks
Chemicals, peptides, and recombinant proteins			
JetPrime transfection reagent	VWR Life Science	Cat#89129-924	
DMEM	Gibco	Cat#11965-092	
Fetal Bovine Serum	Gibco	Cat#16140071	

Penicillin-Streptomycin,	Thermo Fischer Scientific	Cat# 15140122	
Trypsin-EDTA solution	Sigma Aldrich	Cat#T4049	
Phosphate-Buffered Saline	Corning	Cat#21-040-CV	
RIPA Buffer	Sigma Aldrich	Cat#R0278-500ML	
Pierce BCA Protein Assay Kit	ThermoFisher Scientific	Cat#23225	
Mini-PROTEAN TGX Precast Protein Gels	BioRad	Cat#4561096	
Immobilon-P PVDF Membrane	Sigma Aldrich	Cat#IPVH00010	
EveryBlot Blocking Buffer	BioRad	Cat#12010020	
Gemcitabine	MedchemExpress	Cat#HY-17026	
Cisplatin	Millipore Sigma	Cat #232-120-50MG	
Corning® 6.5 mm Transwell® with 8.0 µm Pore Polycarbonate Membrane Insert	Corning	Cat #3422	
Corning® Matrigel® Growth Factor Reduced (GFR) Basement Membrane Matrix	Corning	Cat #356231	
DNase I	Roche	Cat#10104159001	
Liberase TL	Roche	Cat#05401020001	
ACK Lysis Buffer	Life Technologies	Cat # A1049201	

DMSO	Sigma Aldrich	Cat#1371170100	
Naive $CD4^+$ T Cell Isolation Kit, mouse	Miltenyi Biotec	Cat # 130-104-453	
EDTA	Invitrogen	Cat#15575-038	
RPMI 1640	Cytiva	Cat# SH30027.01	
LS columns	Miltenyi Biotec	Cat #130-042-401	
Murine IL-2	Peprotech	Cat # 212-12	
Recombinant Mouse TGF-beta 1	R&D Systems	Cat # 7666-MB-005/CF	
Sodium L-Lactate	Sigma Aldrich	Cat # L7022	
MAGnify™ Chromatin Immunoprecipitation System	Applied Biosystems	Cat # 492024	
Formaldehyde (37% by Weight)	Fisher BioReagents	Cat # BP531-500	
dsDNA HS Assay kit	Invitrogen	Cat # Q32851	
Nuclease-Free Water	Invitrogen	Cat#AM9930	
CD4+CD25+ Regulatory T Cell Isolation Kit, mouse	Miltenyi Biotec	Cat # 130-091-041	
LD columns	Miltenyi Biotec	Cat# 130-042-901	
MS columns	Miltenyi Biotec	Cat# 130-042-201	
AF647 Labeling Kit	Invitrogen	Cat # A20186	

Bovine Serum Albumin	Jackson ImmunoResearch Laboratories	Cat # 001-000-162	
Normal Mouse Serum	Jackson ImmunoResearch Laboratories	Cat # 015-000-120	
Normal Rat Serum	Jackson ImmunoResearch Laboratories	Cat # 012-000-120	
Normal Syrian Hamster Serum	Jackson ImmunoResearch Laboratories	Cat # 007-000-120	
Normal Rabbit Serum	Jackson ImmunoResearch Laboratories	Cat # 011-000-120	
Permeabilization buffer	eBioscience	Cat # 00-8333-56	
Fixation/Permeabilization Diluent	eBioscience	Cat # 00-5223-56	
Fixation/Permeabilization Concentrate	eBioscience	Cat # 00-5123-43	
CellTrace Violet Cell Proliferation Kit	Invitrogen	Cat # C34571	
CellTrace Far Red Cell Proliferation Kit	Invitrogen	Cat # C34572	
CellTrace CFSE Cell Proliferation Kit	Invitrogen	Cat# C34554	

Vybrant DyeCycle Violet Stain	Invitrogen	Cat# V35003	
Live/ Dead Pacific Orange	Invitrogen	Cat # L34968	
Dynabeads™ Mouse T-Activator CD3/CD28	Gibco	Cat # 11456D	
TriZol reagent	Invitrogen	Cat # 15596026	
Chloroform	Sigma-Aldrich	Cat # C2432	
Isopropanol	Sigma-Aldrich	Cat # 19516	
Ethanol	Fisher Chemical	Cat # A4094	
Ethanol	Sigma-Aldrich	Cat # E7023	
ProLong™ Gold Antifade Mountant	Invitrogen	Cat # P36934	
Superscript III cDNA kit	Invitrogen	Cat # 4368814	
SYBR Green Powerup Mastermix	ThermoFisher	Cat # A25742	
pHrodo Red	Invitrogen	Cat # P35372	
L-Lactate Assay Kit	Cayman Chemical	Cat #700510	
Cell-ID 20-Plex Pd Barcoding Kit	Standard BioTools	Cat#201060	
Cell-ID 20 Plex Pd Barcoding Kit	Standard BioTools	Cat#201060	

Paraformaldehyde	ThermoFisher Scientific	Cat# J19943.K2	
10 XF96 Cell Culture Microplates	Agilent Technologies	Cat # 101085-004	
Seahorse XF Real-Time ATP Rate Assay Kit	Agilent Technologies	Cat # 103592-100	
QIAamp DNA Micro Kit	QIAGEN	Cat#56304	
Type-it Microsatellite PCR Kit	QIAGEN	Cat#206243	
Deionized Formamide	Fisher Scientific	Cat# 50-256-001	
GeneScan 500 LIZ dye Size Standard	ThermoFisher Scientific	Cat# 4322682	
Annexin Binding Buffer (5X), for flow cytometry	Invitrogen	Cat#V13246	
Cell ID Cisplatin	Standard BioTools	Cat#201064	
Cell ID Intercalator Ir	Standard BioTools	Cat#201192A	
Agarose	VWR Life Science	Cat#0710-500G	
CUTANA™ Nuclei Extraction Buffer	EpiCypher	Cat#21-1026	
Halt™ Protease Inhibitor Cocktail (100X)	ThermoFisher Scientific	Cat#87786	
QIAprep Spin Miniprep Kit	QIAGEN	Cat#27104	
Plasmid-Safe ATP-Dependent DNase	BIOSEARCH Technologies	Cat#E3101K	

AMPure XP Reagent	BECKMAN COULTER Life Sciences	Cat#A63880	
Exo-Resistant Random Primer	ThermoFisher Scientific	Cat#SO181	
Deoxynucleotide (dNTP) Solution Mix	NEW ENGLAND Biolabs	Cat#N0447L	
phi29 DNA Polymerase	NEW ENGLAND Biolabs	Cat#M0269L	
1kb DNA Ladder	Promega	Cat#G5711	
VECTASHIELD Antifade Mounting Medium with DAPI	Vector Laboratories	Cat#H-1200-10	
BOND Polymer Refine Detection	Leica	Cat#DS9800	
BOND Epitope Retrieval Solution 1	Leica Biosystems	Cat#AR9961	
BOND Wash buffer	Leica Biosystems	Cat#AR9590	
Gamma H2A.X Staining Kit	Abcam	Cat#ab242296	
Etoposide	Abcam	Cat#ab120227	
Poly-D-Lysine	Gibco	Cat#A3890401	
Triton X-100	Sigma-Aldrich	Cat#T8787	
Tween-20	Sigma-Aldrich	Cat#8221840500	
DAPI	Sigma-Aldrich	Cat#10236276001	
Comet Assay Kit	Abcam	Cat#ab238544	
HEPES	Gibco	Cat#15630080	

Lactic Acid	Fisher Chemical	Cat#A159-500	
Sodium L-lactate-3-13C solution	Sigma-Aldrich	Cat#490040	
Histone Purification Mini Kit	Active Motif	Cat#40026	
Perchloric Acid, 70% Solution in Water	Thermo Scientific Chemicals	Cat# 424030010	
Water, LC-MS Grade	Thermo Scientific Chemicals	Ca# 047146.K2	
Acetone, Optima	Fisher Chemical	Cat# A929-1	
Hydrochloric acid, ACS reagent, 37%	Sigma-Aldrich	Cat#320331	
Tetraethylammonium bromide, ReagentPlus, 99%	Sigma-Aldrich	Cat#241059	
Lys-C, Mass Spec Grade	Promega	Cat#VA1170	
DTT (dithiothreitol)	Thermo Scientific	Cat#R0861	
Iodoacetamide	Sigma-Aldrich	Cat#I1149	
Pierce™ Classic IP Kit	Thermo Scientific	Cat# 26146	
Water with 0.1% Formic Acid (v/v), LC/MS Grade	Thermo Scientific	Cat#LS118-500	
Acetonitrile with 0.1% Formic Acid (v/v), LC/MS Grade	Thermo Scientific	Cat#LS120-500	
Oligonucleotides			
Murine sgRNA C1 5'-TAGCATTATCTGCATACC AG -3'	Integrated DNA Technologies. (Exon 4)	N/A	

Murine sgRNA C2 5'- TTCCTCATCACCGAAAG CGG *-3'*	Integrated DNA Technologies. (Exon 1)	N/A	
Murine sgRNA C3 5'- TTCGTAGCAGCGAACAG CCT *-3'*	Integrated DNA Technologies. (Exon 3)	N/A	
Human sgRNAs 5'-GGTATGCAGATAATGCTG AA-3', 5'-ACAGTTTACAGTCTGACT AC-3'	Integrated DNA Technologies. (Exon 4)	N/A	
HuMsh2 Forward 5'-GCAGTTTCATCACTGTCT GCGGT-3'	Integrated DNA Technologies	N/A	
HuMsh2 Reverse 5'-AAGGGCTCTGACTGCTG CAA-3'	Integrated DNA Technologies	N/A	
HuMsh6 Forward 5'-GGAAGAAGAGATGGAGG TAGGCAC-3'	Integrated DNA Technologies	N/A	
HuMsh6 Reverse 5'-TTGGCGGCTACTTCGCC TAGA-3'	Integrated DNA Technologies	N/A	
HuLig3 Forward 5'-GGAGCCGGAGAGGCAG CTAT-3'	Integrated DNA Technologies	N/A	

HuLig3 Reverse 5'-TCACGCCAGTGATGTTTTCGGA-3'	Integrated DNA Technologies	N/A	
HuBaz1b Forward 5'-GCAACTCCCGTGGCAGGAAC-3'	Integrated DNA Technologies	N/A	
HuBaz1b Reverse 5'-TGCTTGCCCCGGATGGTCTT-3'	Integrated DNA Technologies	N/A	
HuExo1 Forward 5'-CTTTCGCGCGCTGTGTAGGC-3'	Integrated DNA Technologies	N/A	
HuExo1 Reverse 5'-ACGACACGTTTCCTTAGGCCTTCC-3'	Integrated DNA Technologies	N/A	
HuLdha Forward 5'-ACGTCGATATTCCTTTTCCACGCT-3'	Integrated DNA Technologies	N/A	
HuLdha Reverse 5'-GCAAGTTCATCTGCCAAGTCCTTCA-3'	Integrated DNA Technologies	N/A	
HuHk2 Forward 5'-TGAGTGGTGGCTCCAAGCCC-3'	Integrated DNA Technologies	N/A	

HuHk2 Reverse 5'-TGACCAAGTGCAGAAGGTTGACCA-3'	Integrated DNA Technologies	N/A	
HuEno2 Forward 5'-CACTGAAGCCATCCAAGCGTGC-3'	Integrated DNA Technologies	N/A	
HuEno2 Reverse 5'-GCACGGGGCACCAGTCTTGA-3'	Integrated DNA Technologies	N/A	
Huβactin Forward 5'-AGCCTCGCCTTTGCCGATCC-3'	Integrated DNA Technologies	N/A	
Huβactin Reverse 5'-ACCATCACGCCCTGGTGCC-3'	Integrated DNA Technologies	N/A	
HuMlh1 ChIP Forward 5'-GCTACGATGAGGCGGCGACA-3'	Integrated DNA Technologies	N/A	
HuMlh1 ChIP Reverse 5'-GTGATCTGGCGCAGAGCGGA-3'	Integrated DNA Technologies	N/A	
HuMsh2 ChIP Forward 5'-ATGCCGGAGAAGCCGACCAC -3'	Integrated DNA Technologies	N/A	

HuMsh2 ChIP Reverse 5'-CACCGCCCACTCTCT GAGGC -3'	Integrated DNA Technologies	N/A	
HuMsh6 ChIP Forward 5'-CCGCCCAAGGCG AAGAACCT -3'	Integrated DNA Technologies	N/A	
HuMsh6 ChIP Reverse 5'-CAACCCCCTGTGCGAGC CT -3'	Integrated DNA Technologies	N/A	
HuLig3 ChIP Forward 5'-AGCCCTGGTTCA TTCTGCTGCG -3'	Integrated DNA Technologies	N/A	
HuLig3 ChIP Reverse 5'-AGTTAGGGTGGA GAGTAA AGTGCGT-3'	Integrated DNA Technologies	N/A	
HuBaz1b ChIP Forward 5'-CGCGACAGTCAT GGAGCGGA-3'	Integrated DNA Technologies	N/A	
HuBaz1b ChIP Reverse 5'-CGCCAC GGGGGAGCAAGTTA-3'	Integrated DNA Technologies	N/A	
HuExo1 ChIP Forward 5'-CCCTCAAGAAGC CGCACGGA-3'	Integrated DNA Technologies	N/A	

HuExo1 ChIP Reverse 5'-CTACACAGCGCG CGAAAGGC-3'	Integrated DNA Technologies	N/A	
HuLdha ChIP Forward 5'-GAGCAGTCTGCC GGTCGGTT-3'	Integrated DNA Technologies	N/A	
HuLdha ChIP Reverse 5'-GCGGGAGGGGCC TTA AGTGG -3'	Integrated DNA Technologies	N/A	
HuHk2 ChIP Forward 5'-GCAGACAGCACC CCACTGTTTG -3'	Integrated DNA Technologies	N/A	
HuHk2 ChIP Reverse 5'-CATGGGATGGGG TGGGTGAGG -3'	Integrated DNA Technologies	N/A	
Mußactin Forward 5'-CCACTGTCGAGTCGCGT CCA -3'	Integrated DNA Technologies.	N/A	
Mußactin Reverse 5'-CACCATCACACCCTGGT GCC -3'	Integrated DNA Technologies	N/A	
MuFoxp3 Forward 5'-AGACCCCTGTGCTCCAA GTG-3'	Integrated DNA Technologies	N/A	

MuFoxp3 Reverse 5'-CAGACTCCATTTGCCAGCAG-3'	Integrated DNA Technologies	N/A	
MuPdcd1 Forward 5'-GCAAGGACGACACTCTGAAGGAGG-3'	Integrated DNA Technologies	N/A	
MuPdcd1 Reverse 5'-CCCCTACGTCCCATGGCCGA-3'	Integrated DNA Technologies	N/A	
MuTgfβ1 Forward 5'-ACCCCCATTGCTGTCCCGTG-3'	Integrated DNA Technologies	N/A	
MuTgfβ1 Reverse 5'-ACGTTTGGGGCTGATCCCGTT-3'	Integrated DNA Technologies	N/A	
MuFoxp3 ChIP Forward 5'-GGGTCAGGGCACTCAGCACA-3'	Integrated DNA Technologies	N/A	
MuFoxp3 ChIP Reverse 5'-AGCTGGCCACTCCTGTAGCCT-3'	Integrated DNA Technologies	N/A	
MuPdcd1 ChIP Forward 5'-TGGGCACGATCCACTATGGCTG -3'	Integrated DNA Technologies	N/A	

MuPdcd1 ChIP Reverse 5'-CCTCCTGATTGGCCGCCCTT-3'	Integrated DNA Technologies	N/A	
MuTgfb1 ChIP Forward 5'-TCCGCAAAGTCTGCCCCTGC -3'	Integrated DNA Technologies	N/A	
MuTgfb1 ChIP Reverse 5'-CTGGCGGCGGAGCACTACTA -3'	Integrated DNA Technologies	N/A	
mBAT-64 Forward 5'-(PET) GCCCACACTCCTGAAAACAGTCAT-3'	ThermoFisher Scientific	N/A	
mBAT-64 Reverse 5'-CCCTGGTGTGGCAACTTTAAGC-3'	Integrated DNA Technologies	N/A	
mBAT-24 Forward 5'-(6FAM) CATAGACCCAGTGCTCATCTTCGT-3'	ThermoFisher Scientific	N/A	
mBAT-24 Reverse 5'-CATTCGGTGGAAAGCTCTGA-3'	Integrated DNA Technologies	N/A	
mBAT-37 Forward 5'-(NED) TCTGCCCAAACGTGCTTAAT-3'	ThermoFisher Scientific	N/A	
mBAT-37 Reverse 5'-CCTGCCTGGGCTAAAATAGA-3'	Integrated DNA	N/A	

	Technologies		
mBAT-59 Forward 5'-(VIC) GTAATCCCTTTATTCCATTTAGCA-3'	ThermoFisher Scientific	N/A	
mBAT-59 Reverse 5'-GGCTCACAACCATCCGTAACAAGA-3'	Integrated DNA Technologies	N/A	
NR21 Forward 5' (VIC) GAGTCGCTGGCACAGTTCTA-3'	ThermoFisher Scientific	N/A	
NR21 Reverse 5'-CTGGTCACTCGCGTTTACAA-3'	Integrated DNA Technologies	N/A	
NR27 Forward 5' (6FAM) AACCATGCTTGCAAACCACT-3'	ThermoFisher Scientific	N/A	
NR27 Reverse 5'-CGATAATACTAGCAATGACC-3'	Integrated DNA Technologies	N/A	
NR24 Forward 5' (PET) GCTGAATTTTACCTCCTGAC-3'	ThermoFisher Scientific	N/A	
NR24 Reverse 5'-ATTGTGCCATTGCATTCCAA-3'	Integrated DNA Technologies	N/A	
BAT-25 Forward 5' (6FAM) TACCAGGTGGCAAAGGGCA-3'	ThermoFisher Scientific	N/A	

BAT-25 Reverse 5'-TCTGCATTTTAACTATGGCTC-3'	Integrated DNA Technologies	N/A	
BAT-26 Forward 5' (NED) CTGCGGTAATCAAGTTTTTAG-3'	ThermoFisher Scientific	N/A	
BAT-26 Reverse 5'-AACCATTCAACATTTTTAACCC-3'	Integrated DNA Technologies	N/A	
Recombinant DNA			
LentiCRISPR v2 vector	AddGene	Cat#52961	
pMD2.G	AddGene	Cat#12259	
pxPAX2-D6V	AddGene	Cat#63586	
psPAX2	AddGene	Cat#12260	
Deposited Data			
IMvigor210 (IMvigor210CoreBiologies R package)	Mariathasan et al., 2018[1]	http://research-pub.gene.com/IMvigor210CoreBiologies	
MSK_2018 dataset	Samstein et al., 2019[2]	https://www.cbioportal.org/study/summary?id=tmb_mskcc_2018	
HCRN dataset	Damrauer et al., 2022[3]	https://www.cbioportal.org/study/summary?id=blca_bcan_hcrn_2022	
blca_msk_tcga_2020	Pietzak et al., 2019[4]	https://www.cbioportal.org/study/summary?id=blca_msk_tcga_2020	
paired_bladder_2022	Clinton et al., 2022[5]	https://www.cbioportal.org/study/clinicalData?id=paired_bladder_2022	
Mouse protein sequence database	Uniprot	https://www.uniprot.org/taxonomy/10090	
Software and algorithms			
FlowJo v10.10	FlowJo, LLC	https://www.flowjo.com/	
Graphpad Prism 10	Graphpad	https://www.graphpad.com/	

Gene Set Enrichment Analysis (GSEA) v4.2.3	Subramanian et al., 2005[6]	http://www.broad.mit.edu/gsea/downloads.jsp	
ImageJ v1.54g	ImageJ	https://imagej.net/ij/	
Circle-Map v.1.1.2	MIT	https://github.com/iprada/Circle-Map	
CNVkit v0.9.10	Apache License, Version 2.0	https://github.com/etal/cnvkit	
circlize v 0.4.15	Zuguang Gu	https://jokergoo.github.io/circlize_book/book/	
Bowtie2 v 2.3.5.1	Langmead et al., 2012[7]	https://github.com/BenLangmead/bowtie2	
FastQC v0.11.9	Simon Andrews	https://github.com/s-andrews/FastQC	
SAMBLASTER v0.1.26	Faust and Hall, 2014[8]	https://github.com/GregoryFaust/samblaster	
SAMTOOLS v1.13	Li et al., 2009[9]	https://www.htslib.org/download/	
SAMBAMBA v0.6.6	Tarasov et al., 2015[10]	https://github.com/biod/sambamba	
MACS2 v2.2.8	Zhang et al., 2008[11]	https://pypi.org/project/MACS2/	
CHIPseeker v1.30.3	Wang et al., 2022[12]	https://bioconductor.org/packages/release/bioc/html/ChIPseeker.html	
clusterProfiler	Yu et al., 2012[13]	https://bioconductor.org/packages/release/bioc/html/clusterProfiler.html	
Manorm v1.1.4	Shao et al., 2012[14]	https://manorm.readthedocs.io/en/v1.1.4/	
deepTools v3.5.1	Ramirez et al., 2016[15]	https://github.com/deeptools/deepTools	
ChromHMM v1.24	Ernst and Kellis, 2017[16]	https://github.com/jernst98/ChromHMM	
STAR v2.7.3a	Alex Dobin[17]	https://github.com/alexdobin/STAR	

Trimmomatic v0.36	Tony Bolger, Bjoern Usadel[18]	https://github.com/usadellab/Trimmomatic	
HTseq v2.0.2	Putri et al., 2022[19]	https://pypi.org/project/HTSeq/	
EdgeR v3.36.0	Robinson et al., 2010[20]	https://bioconductor.org/packages/release/bioc/html/edgeR.html	
BETA v1.0.7	Wang et al., 2013[21]	https://github.com/hanfeisun/BETA	
maftools v2.10.05	Mayakonda et al., 2018[22]	https://github.com/PoisonAlien/maftools	
ggplot2 v3.5.0	Hadley Wickham	https://cran.r-project.org/web/packages/ggplot2/index.html	
R v4.3.2	R Foundation	https://cran.r-project.org/bin/	
Peak Scanner Software v1.0	Applied Biosystems	https://www.thermofisher.com/order/catalog/product/4381867	
Wound healing size tool	Suarez-Arnedo et al., 2020[23]	https://github.com/AlejandraArnedo/Wound-healing-size-tool/wiki	
Aperio eSlide manager v12.4.2.5010	Leica Biosystems	https://www.leicabiosystems.com/digital-pathology/manage/aperio-eslide-manager/	
Colour Deconvolution2	Ruifrok AC, Johnston DA., 2001[24]	https://github.com/landinig/IJ-Colour_Deconvolution2/blob/main/colour_deconvolution2.jar	
Bio-Formats v7.3.1		https://bio-formats.readthedocs.io/en/stable/users/imagej/index.html	
OpenComet v1.3.1	Gyori et al., 2014[25]	https://cometbio.org/index.html	
Seahorse Wave Software v2.6	Agilent	https://www.agilent.com/en/product/cell-analysis/real-time-cell-metabolic-analysis/xf-	

		software/seahorse-wave-desktop-software-740897	
Biorender		https://www.biorender.com/	
Proteome Discoverer v2.4	Thermo Fisher Scientific	https://www.thermofisher.com/us/en/home/industrial/mass-spectrometry/liquid-chromatography-mass-spectrometry-lc-ms/lc-ms-software/multi-omics-data-analysis/proteome-discoverer-software.html#menu1	

Supplementary References:

1. Mariathasan S*, et al.* TGFbeta attenuates tumour response to PD-L1 blockade by contributing to exclusion of T cells. *Nature* **554**, 544-548 (2018).

2. Samstein RM*, et al.* Tumor mutational load predicts survival after immunotherapy across multiple cancer types. *Nat Genet* **51**, 202-206 (2019).

3. Damrauer JS*, et al.* Collaborative study from the Bladder Cancer Advocacy Network for the genomic analysis of metastatic urothelial cancer. *Nat Commun* **13**, 6658 (2022).

4. Pietzak EJ*, et al.* Genomic Differences Between "Primary" and "Secondary" Muscle-invasive Bladder Cancer as a Basis for Disparate Outcomes to Cisplatin-based Neoadjuvant Chemotherapy. *Eur Urol* **75**, 231-239 (2019).

5. Clinton TN*, et al.* Genomic heterogeneity as a barrier to precision oncology in urothelial cancer. *Cell Rep* **41**, 111859 (2022).

6. Subramanian A*, et al.* Gene set enrichment analysis: a knowledge-based approach for interpreting genome-wide expression profiles. *Proc Natl Acad Sci U S A* **102**, 15545-15550 (2005).

7. Langmead B, Salzberg SL. Fast gapped-read alignment with Bowtie 2. *Nat Methods* **9**, 357-359 (2012).

8. Faust GG, Hall IM. SAMBLASTER: fast duplicate marking and structural variant read extraction. *Bioinformatics* **30**, 2503-2505 (2014).

9. Li H*, et al.* The Sequence Alignment/Map format and SAMtools. *Bioinformatics* **25**, 2078-2079 (2009).

10. Tarasov A, Vilella AJ, Cuppen E, Nijman IJ, Prins P. Sambamba: fast processing of NGS alignment formats. *Bioinformatics* **31**, 2032-2034 (2015).

11. Zhang Y*, et al.* Model-based analysis of ChIP-Seq (MACS). *Genome Biol* **9**, R137 (2008).

12. Wang Q*, et al.* Exploring Epigenomic Datasets by ChIPseeker. *Curr Protoc* **2**, e585 (2022).

13. Yu G, Wang LG, Han Y, He QY. clusterProfiler: an R package for comparing biological themes among gene clusters. *OMICS* **16**, 284-287 (2012).

14. Shao Z, Zhang Y, Yuan GC, Orkin SH, Waxman DJ. MAnorm: a robust model for quantitative comparison of ChIP-Seq data sets. *Genome Biol* **13**, R16 (2012).

15. Ramirez F*, et al.* deepTools2: a next generation web server for deep-sequencing data analysis. *Nucleic Acids Res* **44**, W160-165 (2016).

16. Ernst J, Kellis M. Chromatin-state discovery and genome annotation with ChromHMM. *Nat Protoc* **12**, 2478-2492 (2017).

17. Dobin A*, et al.* STAR: ultrafast universal RNA-seq aligner. *Bioinformatics* **29**, 15-21 (2013).

18. Bolger AM, Lohse M, Usadel B. Trimmomatic: a flexible trimmer for Illumina sequence data. *Bioinformatics* **30**, 2114-2120 (2014).

19. Putri GH, Anders S, Pyl PT, Pimanda JE, Zanini F. Analysing high-throughput sequencing data in Python with HTSeq 2.0. *Bioinformatics* **38**, 2943-2945 (2022).

20. Robinson MD, McCarthy DJ, Smyth GK. edgeR: a Bioconductor package for differential expression analysis of digital gene expression data. *Bioinformatics* **26**, 139-140 (2010).

21. Wang S*, et al.* Target analysis by integration of transcriptome and ChIP-seq data with BETA. *Nat Protoc* **8**, 2502-2515 (2013).

22. Mayakonda A, Lin DC, Assenov Y, Plass C, Koeffler HP. Maftools: efficient and comprehensive analysis of somatic variants in cancer. *Genome Res* **28**, 1747-1756 (2018).

23. Suarez-Arnedo A, Torres Figueroa F, Clavijo C, Arbelaez P, Cruz JC, Munoz-Camargo C. An image J plugin for the high throughput image analysis of in vitro scratch wound healing assays. *PLoS One* **15**, e0232565 (2020).

24. Ruifrok AC, Johnston DA. Quantification of histochemical staining by color deconvolution. *Anal Quant Cytol Histol* **23**, 291-299 (2001).

25. Gyori BM, Venkatachalam G, Thiagarajan PS, Hsu D, Clement MV. OpenComet: an automated tool for comet assay image analysis. *Redox Biol* **2**, 457-465 (2014).